Research Article Vol. 58, No. 5 / 10 February 2019 / Applied Optics A13

applied optics

Fast method for ringing artifacts reduction in random phase-free kinoforms

Chun Chen,[1] Jun Wang,[1,*] Dan Xiao,[1] and Qiong-Hua Wang[2]

[1]School of Electronics and Information Engineering, Sichuan University, Chengdu 610065, China
[2]School of Instrumentation and Optoelectronic Engineering, Beihang University, Beijing 100083, China
*Corresponding author: jwang@scu.edu.cn

Received 21 August 2018; revised 15 October 2018; accepted 16 October 2018; posted 17 October 2018 (Doc. ID 342881); published 9 November 2018

In holographic projection, ringing artifacts and degradation appear when the speckle noise problem is solved based on the random phase-free method. In this paper, we present a fast method to suppress the ringing artifacts in random phase-free kinoforms. We first reduce the distance between the hologram plane and the focal plane, and keep the focal length of the convergence light unchanged in the random phase-free method. Next, the complex amplitude is modulated using a single spatial light modulator. Consequently, the ringing artifacts and speckle noise reduction in the reconstructed image can be achieved. At the same time, the computing speed can be increased with our proposed method. Numerical simulations and optical experiments have validated the feasibility of the proposed method.

https://doi.org/10.1364/AO.58.000A13

1. INTRODUCTION

In recent years, laser projector displays have become more and more attractive due to their high-contrast, wide color gamut images, and low power consumption [1,2]. One of the major projector display methods is holographic projection, which is based on computer-generated holography (CGH). The method can achieve color projection with a single spatial light modulator (SLM) device and also has potential in three-dimensional (3D) scene projection [3,4]. However, the size of optical zoom system in holographic projection is a problem. To reduce the system size, a promising technology of holographic projection has been proposed [5], which can achieve zoomable projection without a zoom lens. However, since the original image is multiplied by a random phase, the reconstructed image is contaminated by speckle noise.

To solve the problem of speckle noise, many methods have been proposed, such as the iterative CGH algorithm [6–8], time-integrating method [9,10], multirandom phase method [11], error diffusion method [12,13], down-sampling method [14], and light-emitting diode (LED) illumination method [15]. However, there are still some problems, which include a long calculation time and the need for an SLM with a high frame rate. More recently, a non-iterative algorithm called random phase-free method [16] has been proposed. It uses virtual convergence light instead of random phase to spread the object light. Based on this method, speckle noise can be reduced, and the image quality also can be improved. Although this method is useful in speckle noise suppression, the reconstructed image is contaminated by ringing artifacts. The iterative random phase-free method [17] has been proposed to suppress ringing artifacts, which combines the random phase-free method and the Gerchberg–Saxton (GS) algorithm. Moreover, the amplitude inverse filter method and the phase porting method [18] have been proposed as fast methods to reduce ringing artifacts, both of which use the characteristics of the ringing artifacts to solve this problem. Those methods are effective in reducing ringing artifacts, but have some limitations that restrict their application, including a long calculation time and a complex procedure.

In this paper, we propose a fast, simple method to reduce ringing artifacts in random phase-free kinoforms. Furthermore, we also analyze the reasons for ringing artifacts. The method reduces the distance between the hologram plane and the focal plane but does not change the focal length of the virtual convergence light in the random phase-free method. In this way, ringing artifacts can be effectively suppressed. In addition, the aliasing-reduced shifted and scaled (ARSS) Fresnel diffraction algorithm [19] is used to calculate the diffraction field behind the focal plane, allowing the effective information to be separated by one spatial filter [20,21]. And off-axis double-phase method [22] is applied to achieve complex amplitude modulation using a single SLM. Finally, we can reduce speckle noise and ringing artifacts with the proposed method.

2. RANDOM PHASE-FREE KINOFORM

Figure 1 shows the geometrical among the image plane, hologram plane, and virtual convergence light in the random phase-free method. In this method, the diffraction field in the

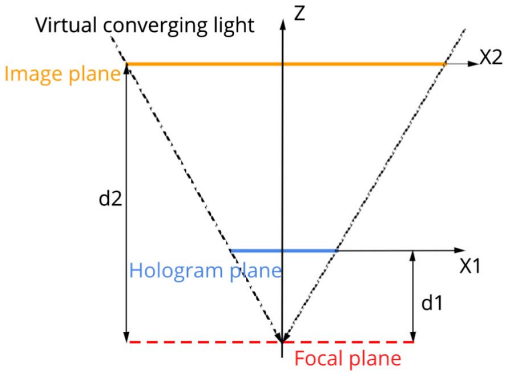

Fig. 1. Geometrical relation among the image plane, hologram plane, and virtual convergence light in the random phase-free method.

hologram plane is calculated using the ARSS–Fresnel diffraction, since the sizes of the image plane and hologram plane are different. Because the size of the image plane is larger than the hologram plane, the random phase is usually used to spread the object light to the hologram plane. However, the random phase will cause random phase distribution in the reconstructed image, and speckle noise will appear. In the random phase-free method, the virtual convergence light is used to spread object light instead of the random phase. Based on this method, the speckle noise can be reduced in the reconstructed image. To separate the effective information from higher-order diffraction light using a spatial filter in the random phase-free method, the diffraction field behind the focal plane must be calculated. Figure 2 shows the geometrical relation of the random phase-free kinoform-generating method. The difference between these two methods is that the hologram plane is placed before and behind the focal plane, as shown in Figs. 1 and 2, respectively. In addition, the second method can filter the effective information more easily during the kinoform reconstruction.

In Fig. 2, d_1 and d_2 represent the distance from the focal plane to the hologram plane and the image plane, respectively. The relationship between d_1 and d_2 is $d_2 = d_1 \cdot s$. s is the scaling factor, which means that the sampling pitch and the reconstructed image size on the image plane will be affected by this parameter. The scaling factor s is usually set to a number which

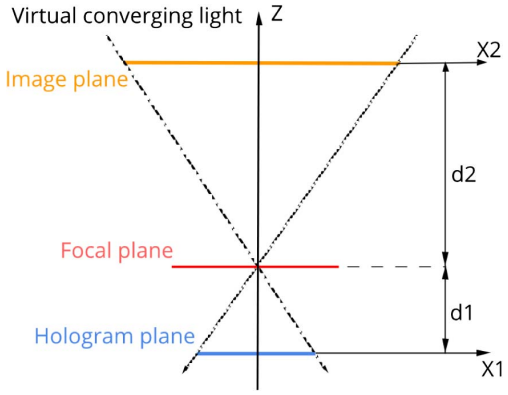

Fig. 2. Geometrical relation among the image plane, hologram plane, focal plane, and virtual convergence light in the random phase-free kinoform-generating method.

is larger than 1. The diffraction distance from image plane to hologram plane is denoted by z, and $z = d_1 + d_2$, assuming that $A(x_2, y_2)$ represents the amplitude of the input image. Before calculation, the image is multiplied by a virtual convergence light given by $w(x_2, y_2)$, which can be expressed as

$$w(x_2, y_2) = \exp(-i\pi(s^2x_2^2 + t^2y_2^2)/\lambda d_2), \tag{1}$$

where λ is the wavelength of light, t is the scaling factor on the y axis, and $t = s$. The complex amplitude of the image plane is accordingly expressed by $u_2(x_2, y_2) = A(x_2, y_2) \cdot w(x_2, y_2)$. The diffraction field in the hologram plane is directly calculated by the ARSS–Fresnel diffraction algorithm, which is given as

$$\begin{aligned} u_1(x_1, y_1) &= C_z \iint u_2(x_2, y_2) \\ &\quad \cdot \exp\left\{\frac{i\pi}{\lambda z}[(x_1 - sx_2)^2 + (y_1 - ty_2)^2]\right\} \mathrm{d}x_2 \mathrm{d}y_2 \\ &= C_z \mathrm{FFT}^{-1}\{\mathrm{FFT}[u_2(x_2, y_2) \cdot \exp(i\varphi_u)] \\ &\quad \cdot \mathrm{FFT}[\exp(i\varphi_h)]\}, \end{aligned} \tag{2}$$

where FFT[·] and FFT^{-1}[·] represent the fast Fourier transform (FFT) operation and inverse FFT operation, respectively. φ_u and φ_h are quadratic phase factors, and C_z is constant phase factor. The 1D expressions are given in Eq. (8), and more details can be found in Ref. [19]. Δx_1, Δy_1 denote the sampling pitch on the hologram plane, $s \cdot \Delta x_2$, $t \cdot \Delta y_2$ denote the sampling pitch on the image plane, and $\Delta x_1 = \Delta x_2$, $\Delta y_1 = \Delta y_2$.

The off-axis double-phase method is applied as an encoding procedure, and the complex amplitude $u_1(x_1, y_1)$ can be decomposed into two pure phase values, $\theta_1(x_1, y_1)$ and $\theta_2(x_1, y_1)$. The expressions can be written as

$$\begin{aligned} \theta_1(x_1, y_1) &= \varphi_1(x_1, y_1) + \cos^{-1}[A_1(x_1, y_1)/A_{\max}], \\ \theta_2(x_1, y_1) &= \varphi_1(x_1, y_1) - \cos^{-1}[A_1(x_1, y_1)/A_{\max}], \end{aligned} \tag{3}$$

where φ_1 and $A_1(x_1, y_1)$ represent the phase and amplitude of $u_1(x_1, y_1)$, respectively. $A_{\max}$ is the maximum value of $A_1(x_1, y_1)$. The final expression of the random phase-free kinoform is given by [22]

$$\begin{aligned} u_d(x_1, y_1) &= \theta_1(x_1, y_1)M_1(x_1, y_1) + \theta_2(x_1, y_1)M_2(x_1, y_1) \\ &\quad + 2\pi x_1 \sin \alpha/\lambda, \end{aligned} \tag{4}$$

where α is the blaze angle of a blazing grating in x_1-direction, and M_1 and M_2 are the complementary 2D binary gratings (checkerboard patterns), and their expressions are given as

$$M_1(i \cdot dx_1, j \cdot dy_1) = \begin{cases} 0 & (i \cdot j \text{ are odd or even}) \\ 1 & (\text{else}) \end{cases}, \tag{5}$$

$$M_2(i \cdot dx_1, j \cdot dy_1) = \begin{cases} 1 & (i \cdot j \text{ are odd or even}) \\ 0 & (\text{else}) \end{cases}. \tag{6}$$

Figure 3 shows the numerical results from the random phase-free kinoform. Figures 3(a) and 3(b) show the original image and the reconstructed image, respectively. It's clear that the ringing artifacts appeared in the reconstructed image. In the following section, we present an effective method to reduce the ringing artifacts, and the reasons for ringing artifacts are also analyzed.

(a) (b)

Fig. 3. Computer simulation results. (a) Original image and (b) reconstructed image from random phase-free kinoform.

3. PROPOSED METHOD

The scheme of the proposed method is shown in Fig. 4. ① and ② represent the original and changed positions of hologram plane, respectively. The moved distance is Δd.

When the hologram plane moves toward the focal plane but the focal length of the virtual convergence light does not change, the ringing artifacts can be reduced in the reconstructed image. The reason analysis is below.

For simplicity, the analysis of ringing artifacts is based on the 1D ARSS–Fresnel diffraction algorithm. Because Fresnel diffraction allows the separation of variables, it's easy to extend to 2D ARSS–Fresnel diffraction. The 1D expression is given as

$$\begin{aligned} u_1(x_1) &= C_z \int A(x_2)\cdot w(x_2)\cdot \exp\left\{\frac{i\pi}{\lambda z}[(x_1 - sx_2)^2]\right\} \mathrm{d}x_2 \\ &= C_z \mathrm{FFT}^{-1}\{\mathrm{FFT}[A(x_2)\cdot w(x_2)\cdot \exp(i\varphi_u)] \\ &\quad \cdot \mathrm{FFT}[\exp(i\varphi_h)]\}, \end{aligned} \tag{7}$$

where the C_z, $w(x_2)$, $\exp(i\varphi_u)$, and $\exp(i\varphi_h)$ are defined by

$$\begin{aligned} C_z &= \frac{\exp\left(ikz + \frac{i\pi}{\lambda z}(1-s)x_1^2\right)}{i\lambda z} \\ w(x_2) &= \exp\left(-\frac{i\pi}{\lambda d_2}s^2 x_2^2\right) \\ \exp(i\varphi_u) &= \exp\left(\frac{i\pi}{\lambda z}(s^2 - s)x_2^2\right) \\ \exp(i\varphi_h) &= \exp\left(\frac{i\pi}{\lambda z}sx_2^2\right), \end{aligned} \tag{8}$$

where $x_1 = \Delta x_1 \cdot m$ and $x_2 = \Delta x_2 \cdot m$, and m is integer with ranges of $m \in [-N/2, N/2 - 1]$, where N is the number of sampling points. Assuming $U_f = \mathrm{FFT}[A(x_2)\cdot w(x_2)\cdot \exp(i\varphi_u)]$ and $H_f = \mathrm{FFT}[\exp(i\varphi_h)]$, the $u_1(x_1)$ can be rewritten as $u_1(x_1) = C_z \mathrm{FFT}^{-1}\{U_f \cdot H_f\}$. Here, U_f contains most of the information about the input signal $A(x_2)$, and H_f is the transfer function in ARSS–Fresnel diffraction algorithm. In the following section, we will calculate the amplitude distribution of U_f, H_f, and the reconstructed signal in different d_1. The calculation results are then used to analysis the reasons for ringing artifacts in the reconstructed signal.

The calculation parameters are $N = 2048$, $\lambda = 532.0$ nm, $\Delta x_1 = \Delta x_2 = 8.0$ μm, and $s = 3$. When the hologram plane is at the position ①, we get $z = 1.6$ m, $d_1 = 0.4$ m, and $d_2 = 1.2$ m. Figures 5(a) and 5(b) show the original input signal and the amplitude distribution of U_f and H_f, respectively. After the ARSS–Fresnel diffraction calculation, the amplitude distribution of U_1 in the hologram plane is shown in Fig. 5(c). Figure 5(d) shows the reconstructed signal A_r from the diffraction field.

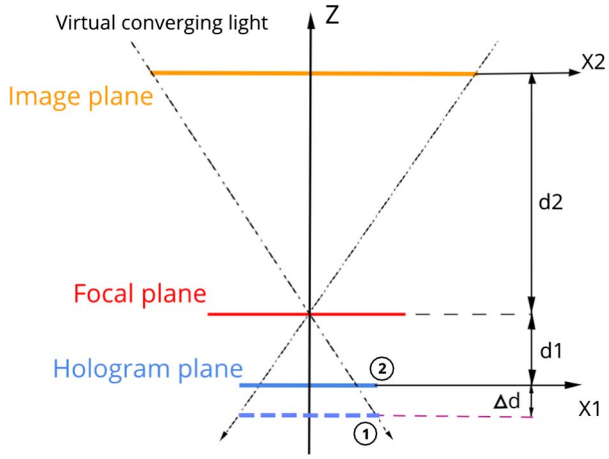

Fig. 4. Geometrical relation among image plane, hologram plane, focal plane, and virtual convergence light in the proposed method.

In Fig. 5(d), the reconstructed signal A_r is contaminated by ringing artifacts. The reason is that the amplitude distribution of transfer function H_f is fluctuant, and the bandwidth of H_f is almost the same as U_f. The amplitude fluctuation in the edge of H_f will influence the amplitude of U_f, which causes the ringing artifacts in the reconstructed signal A_r. As shown in Fig. 5(d), the fluctuation is small in the center area of H_f. If you suppose that the bandwidth of U_f is smaller than H_f, the amplitude influence caused by H_f in U_f will be reduced. Therefore, the ringing artifacts in the reconstructed signal A_r will be suppressed.

Figures 6(a) and 6(b) show the amplitude distribution of U_f, H_f, and A_r at $d_1 = 0.3$ m and $d_1 = 0.2$ m, respectively. When the hologram plane is moved close to the focal plane, the bandwidth of H_f becomes larger than U_f. Thus in U_f, the amplitude influence caused by H_f becomes smaller. Therefore, the ringing artifacts in the reconstructed signal are reduced.

When $d_1 = 0$ m, the hologram plane position is at the focal plane. Figures 7(a) and 7(b) show the amplitude distribution of U_f, H_f, and A_r, respectively. The bandwidth of H_f is much

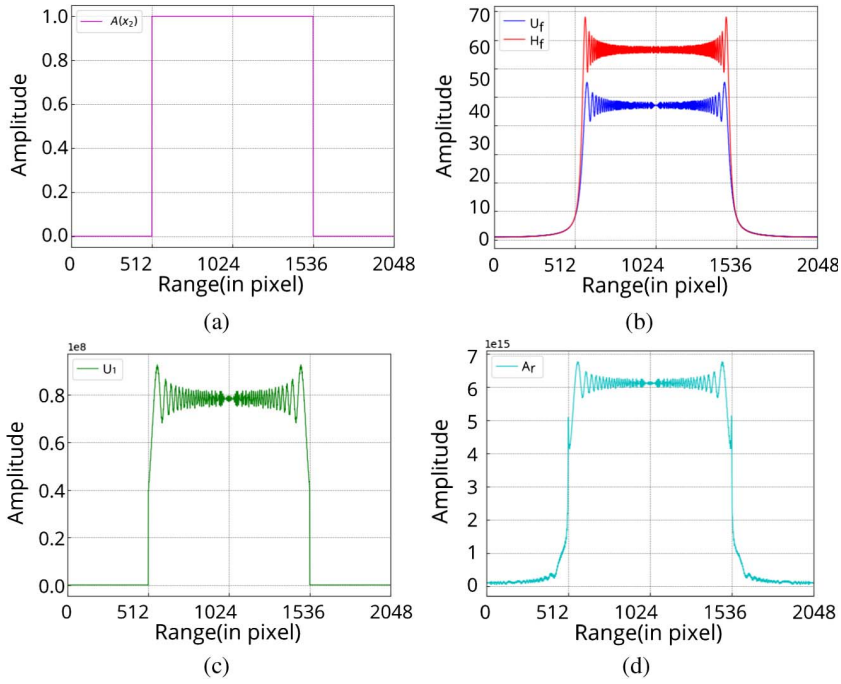

Fig. 5. Amplitude distribution: (a) $A(x_2)$, (b) U_f, H_f, (c) U_1, and (d) A_r.

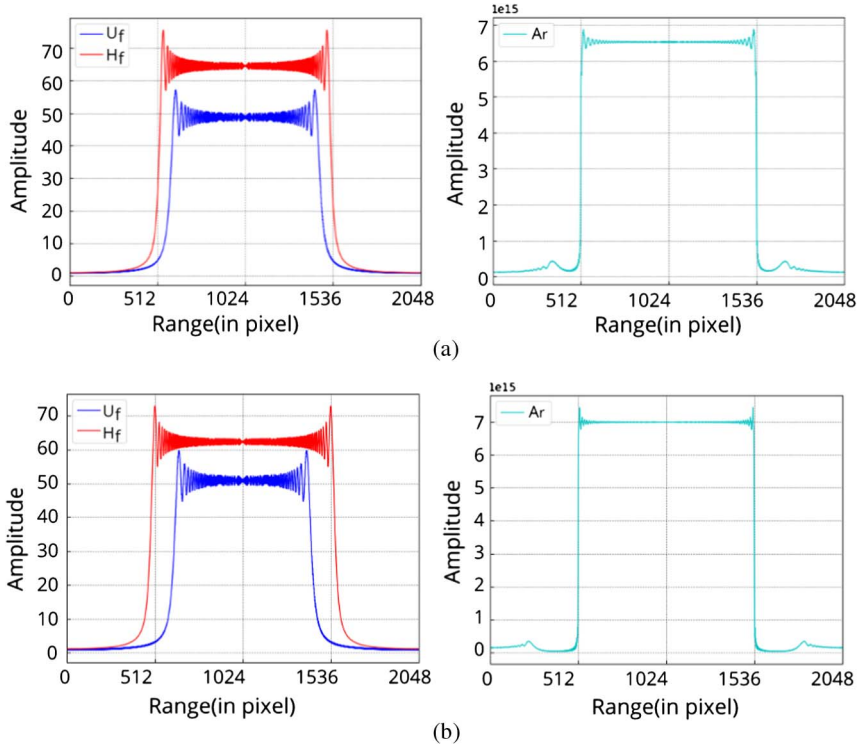

Fig. 6. Amplitude distribution of U_f, H_f, and A_r: (a) $d_1 = 0.3$ m and (b) $d_1 = 0.2$ m.

larger than U_f; thus, the ringing artifacts in the reconstructed signal are reduced. However, if the Rect function is used to band-limit $\exp(i\varphi_h)$ [19] to reduce the aliasing error, the ringing artifacts will appear in A_r. The band-limited area in the pixel units of $\exp(i\varphi_h)$ is given as

$$|n_h| \le \left| \frac{\lambda z}{2s\Delta x_1^2} \right|, \tag{9}$$

where $|n_h|$ is the number of pixels in the band-limited area, which, in this case, is $|n_h| \le 1662$. In numerical simulations,

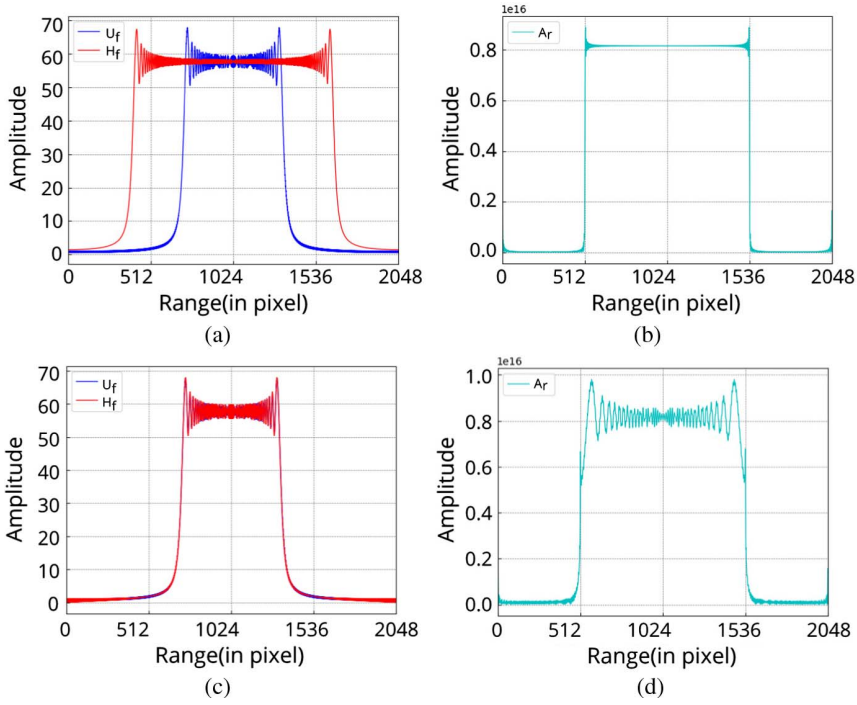

Fig. 7. Amplitude distribution: (a) U_f, H_f, and (b) reconstructed signal A_r (no band-limit), (c) band-limited U_f, H_f, and (d) reconstructed signal A_r (band-limit).

when we set the band-limited area to $[-N/4, N/4]$, the number of pixels in the band-limited area is 1024, which meets the condition. The expression of the band-limited function can be written as

$$\mathrm{Rect}(n) = \begin{cases} 1 & (512 \le n \le 1536) \\ 0 & (\mathrm{else}) \end{cases}, \tag{10}$$

where n is an integer with ranges of $n \in [0, N]$. Figure 7(d) shows the reconstructed signal through the band-limit operation, and the ringing artifacts appeared. The reason is that the bandwidth of H_f is the same as U_f, which is shown in Fig. 7(c). In U_f, the amplitude influence caused by H_f is strong. Therefore, the ringing artifacts appeared in the reconstructed signal.

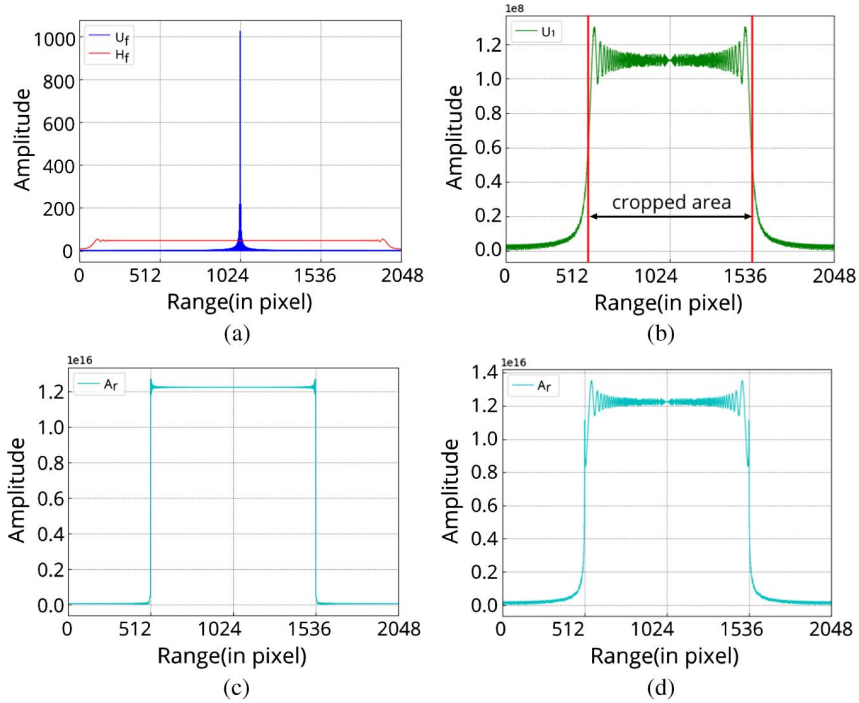

Fig. 8. Amplitude distribution: (a) U_f, H_f, (b) U_1, (c) reconstructed signal A_r, and (d) reconstructed signal A_r from the cropped diffraction field U_1.

When the hologram plane moves over the focal plane (the schematic is shown in Fig. 1), we get $d_1 = 0.4$ m, $d_2 = 1.2$ m, and $z = d_2 - d_1 = 0.8$ m. Figures 8(a), 8(b), and 8(c) show the amplitude distribution of U_f, H_f, U_1, and A_r, respectively. The bandwidth of H_f is much larger than U_f, and the ringing artifacts are reduced in the reconstructed signal. However, if the Rect function is used to band-limit C_z or directly crop the diffraction field, the result of these two operations is equal. The operations will crop the high spatial frequency of the diffraction field. In Fig. 8(b), the red line area shows the amplitude distribution of the cropped diffraction field. Because the high spatial frequency in the diffraction field is cropped, the Gibbs phenomenon [23] can be observed in the reconstructed signal. Thus, the ringing artifacts appeared in the reconstructed signal. Figure 8(d) shows the reconstructed signal from the cropped diffraction field.

As can be seen from the above analysis, there are two main reasons for ringing artifacts. The first reason is that the high spatial frequency of the diffraction field is cropped. Another reason is that the signal frequency domain is influenced by the transfer function H_f. In the original method shown in Fig. 2, the reasons for the ringing artifacts are that the bandwidth of U_f is almost the same as H_f, and the high spatial frequency of the diffraction field is cropped. By reducing the distance between the hologram plane and the focal plane, the proposed method can reduce the influence of the transfer function in U_f and also can shrink the diffraction field to avoid cropping the high spatial frequency. In that way, the high spatial frequency of the original image can be preserved.

Table 1. Numerical Reconstruction Conditions

	Proposed Method	Iterative Method
CGH resolution $M \times N$	1920 × 1080	1920 × 1080
CGH pixel pitch Δx_1	8.0 μm	8.0 μm
Wavelength λ	532.0 nm	532.0 nm
d_1	0.21 m	0.3 m
d_2	0.9 m	0.9 m
Scaling factor s	3.0	3.0
Number of iterations	0	4

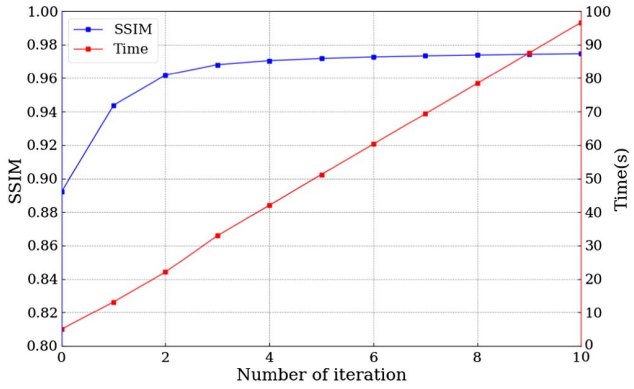

Fig. 10. SSIM and calculation time of the iterative method with a different number of iterations.

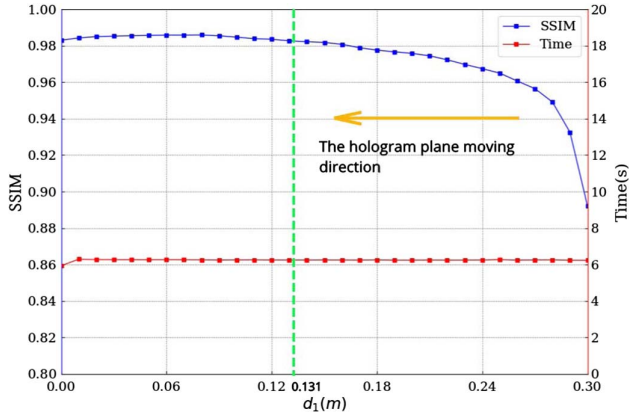

Fig. 11. SSIM and calculation time of the proposed method with a different d_1.

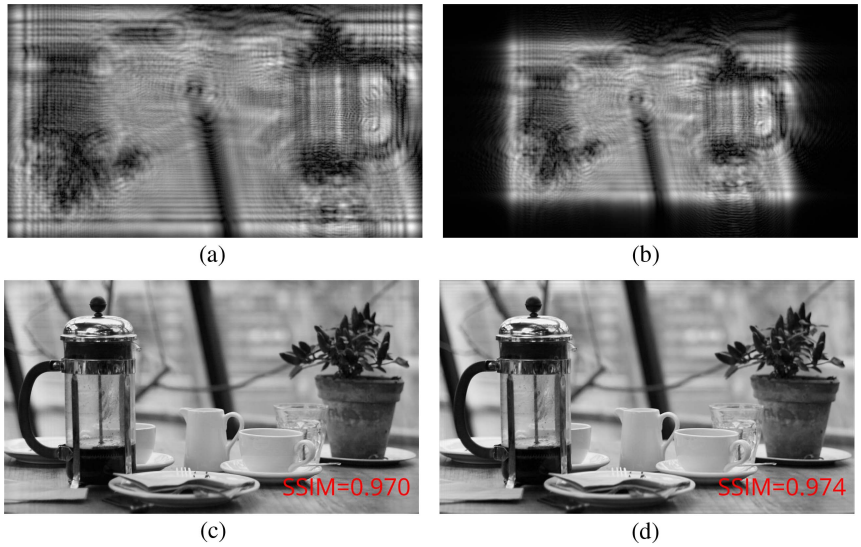

(a) (b) (c) (d)

Fig. 9. Numerical simulations: (a) diffraction intensity in the hologram plane by the iterative method, and (b) the proposed method. (c) Reconstructed image by the iterative method and (d) the proposed method.

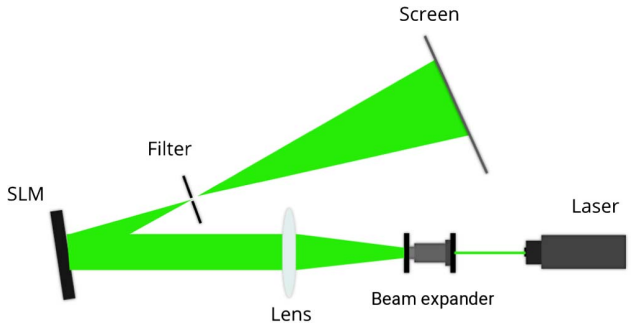

Fig. 12. Optical system.

Table 2. Optical Experimental Conditions

	Original Method	Proposed Method	Iterative Method
SLM resolution	1920 × 1080	1920 × 1080	1920 × 1080
SLM pixel pitch	8.0 μm	8.0 μm	8.0 μm
Wavelength	532.0 nm	532.0 nm	532.0 nm
d_1	0.3 m	0.21 m	0.3 m
d_2	0.9 m	0.9 m	0.9 m
Scaling factor s	3.0	3.0	3.0
Number of iterations	0	0	4

Thus, the ringing artifacts in the reconstructed image can be reduced.

4. RESULTS

A. Numerical Simulations

The numerical reconstruction conditions are given in Table 1. Figures 9(a) and 9(b) show the diffraction intensity distribution in the hologram plane by the iterative method and the proposed method, respectively. Figures 9(c) and 9(d) show the reconstructed image by the iterative method and the proposed method, respectively. In Fig. 9(b), as the hologram plane is moved, the diffraction field is shrunk. Thus, the high spatial frequency can avoid the crop operation, and the ringing artifacts are reduced in the reconstructed image, as shown in Fig. 9(d).

As usual, the structural similarity (SSIM) is used to measure image quality, and the details can be found in Ref. [24]. Figure 10 shows the reconstructed image quality and the calculation time of the iterative method with a different number of iterations. The calculation time for the iterative method is increased linearly according to the number of iterations. Figure 11 shows the reconstructed image quality of the proposed method with a different d_1. When d_1 becomes smaller the reconstructed image quality becomes better. The

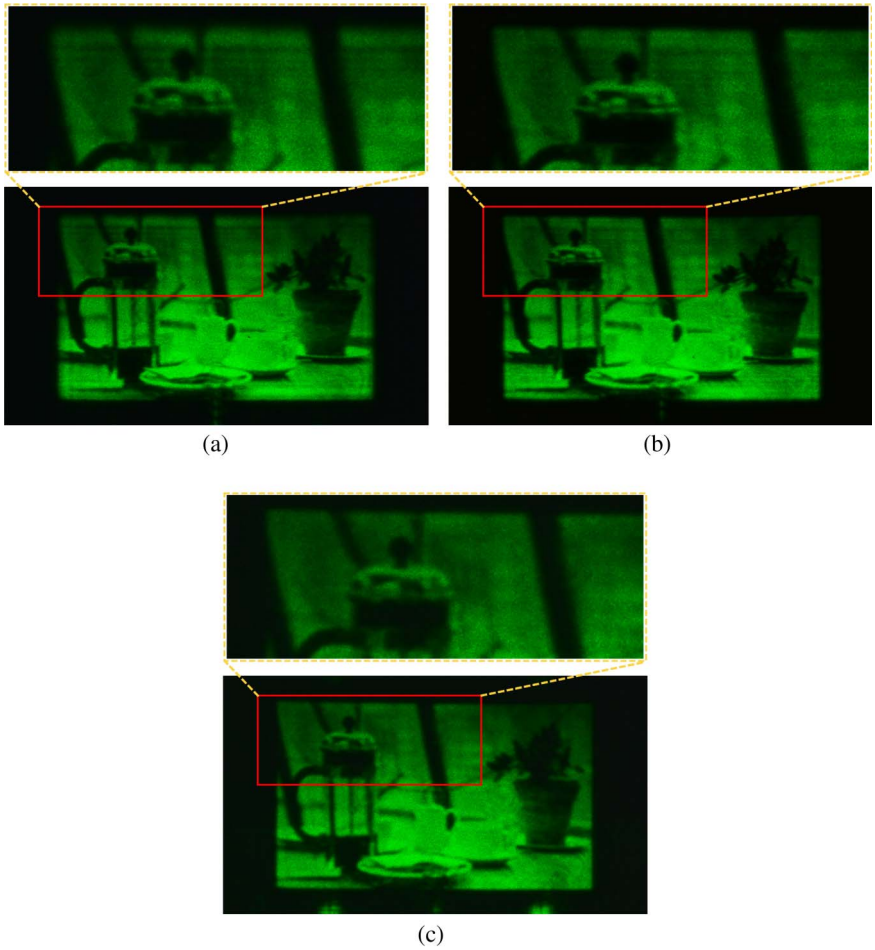

Fig. 13. Optical reconstructed images: (a) from the original method, (b) from the iterative method, and (c) from the proposed method.

calculation time of the proposed method almost does not change with a different d_1, and is equal to the time of the original method.

As shown in Fig. 11, although d_1 can be reduced to 0 m in the numerical simulation, the virtual convergence light focal point should be separated from zero order light in the optical reconstruction. The maximum diffraction angle of SLM limits d_1; thus, the minimal value of d_1 is determined by

$$d_{1\,\min} = \Delta x_1 \times N/2/(\sin^{-1}(\lambda/2\Delta x_1)). \tag{11}$$

In this case, $d_{1\,\min} \simeq 0.131$ m. Above this distance, the reconstructed image can be separated from zero order light in the optical reconstruction.

B. Optical Experiments

The optical system of reconstruction is shown in Fig. 12, and the conditions of optical reconstruction are given in Table 2.

Figure 13 shows the optical experiments results. Figure 13(a) is the reconstructed image by the original method, and the red box indicates the interesting area, in which the ringing artifacts are observed. Figures 13(b) and 13(c) show the reconstructed images by the iterative method and the proposed method, respectively. The results show that the ringing artifacts are reduced by the proposed method.

5. CONCLUSION

We present a fast, simple method to reduce ringing artifacts in random phase-free kinoforms in this paper, and also analyze the reasons that cause the ringing artifacts. Compared to the iterative method, the proposed method needs no additional calculation time and can also achieve good image quality in a simple way. Because the analysis of ringing artifacts is based on the ARSS–Fresnel diffraction algorithm, the proposed method is applicable to both random phase-free kinoforms and random phase-free amplitude CGHs. Therefore, the proposed method can be easily used to reduce ringing artifacts in lensless zoomable holographic projection based on the random phase-free method.

Funding. National Key Research and Development Program of China (2017YFB1002900); National Natural Science Foundation of China (NSFC) (61320106015); Sichuan Science and Technology Program (2018GZ0533).

REFERENCES

1. E. Buckley, "Holographic projector using one lens," Opt. Lett. **35**, 3399–3401 (2010).
2. E. Buckley, "Holographic laser projection," J. Disp. Technol. **7**, 135–140 (2011).
3. F. Yaraş, H. Kang, and L. Onural, "State of the art in holographic displays: a survey," J. Disp. Technol. **6**, 443–454 (2010).
4. Y. Zhao, L. Cao, H. Zhang, D. Kong, and G. Jin, "Accurate calculation of computer-generated holograms using angular-spectrum layer-oriented method," Opt. Express **23**, 25440–25449 (2015).
5. T. Shimobaba, M. Makowski, T. Kakue, M. Oikawa, N. Okada, Y. Endo, R. Hirayama, and T. Ito, "Lensless zoomable holographic projection using scaled Fresnel diffraction," Opt. Express **21**, 25285–25290 (2013).
6. M. Makowski, M. Sypek, A. Kolodziejczyk, and G. Mikula, "Three-plane phase-only computer hologram generated with iterative Fresnel algorithm," Opt. Eng. **44**, 125805 (2005).
7. R. W. Gerchberg, "A practical algorithm for the determination of phase from image and diffraction plane pictures," Optik **35**, 237–246 (1972).
8. J. R. Fienup, "Reconstruction of an object from the modulus of its Fourier transform," Opt. Lett. **3**, 27–29 (1978).
9. Y. Takaki and M. Yokouchi, "Speckle-free and grayscale hologram reconstruction using time-multiplexing technique," Opt. Express **19**, 7567–7579 (2011).
10. M. Makowski, "Minimized speckle noise in lens-less holographic projection by pixel separation," Opt. Express **21**, 29205–29216 (2013).
11. J. Amako, H. Miura, and T. Sonehara, "Speckle-noise reduction on kinoform reconstruction using a phase-only spatial light modulator," Appl. Opt. **34**, 3165–3171 (1995).
12. R. Eschbach, "Comparison of error diffusion methods for computer-generated holograms," Appl. Opt. **30**, 3702–3710 (1991).
13. P. W. M. Tsang and T.-C. Poon, "Novel method for converting digital Fresnel hologram to phase-only hologram based on bidirectional error diffusion," Opt. Express **21**, 23680–23686 (2013).
14. P. W. M. Tsang, Y.-T. Chow, and T. C. Poon, "Generation of phase-only Fresnel hologram based on down-sampling," Opt. Express **22**, 25208–25214 (2014).
15. F. Yaraş, H. Kang, and L. Onural, "Real-time phase-only color holographic video display system using LED illumination," Appl. Opt. **48**, H48–H53 (2009).
16. T. Shimobaba and T. Ito, "Random phase-free computer-generated hologram," Opt. Express **23**, 9549–9554 (2015).
17. T. Shimobaba, T. Kakue, Y. Endo, R. Hirayama, D. Hiyama, S. Hasegawa, Y. Nagahama, M. Sano, M. Oikawa, T. Sugie, and T. Ito, "Improvement of the image quality of random phase-free holography using an iterative method," Opt. Commun. **355**, 596–601 (2015).
18. Y. Nagahama, T. Shimobaba, T. Kakue, N. Masuda, and T. Ito, "Speeding up image quality improvement in random phase-free holograms using ringing artifact characteristics," Appl. Opt. **56**, F61–F66 (2017).
19. T. Shimobaba, T. Kakue, N. Okada, M. Oikawa, Y. Yamaguchi, and T. Ito, "Aliasing-reduced Fresnel diffraction with scale and shift operations," J. Opt. **15**, 075405 (2013).
20. C. Chang, Y. Qi, J. Wu, J. Xia, and S. Nie, "Speckle reduced lensless holographic projection from phase-only computer-generated hologram," Opt. Express **25**, 6568–6580 (2017).
21. C. Liu and D. Wang, "Light intensity and FOV-controlled adaptive fluidic iris," Appl. Opt. **57**, D27–D31 (2018).
22. Y. Qi, C. Chang, and J. Xia, "Speckleless holographic display by complex modulation based on double-phase method," Opt. Express **24**, 30368–30378 (2016).
23. D. Gottlieb and C. Shu, "On the Gibbs phenomenon and its resolution," SIAM Rev. **39**, 644–668 (1997).
24. Z. Wang, A. C. Bovik, H. R. Sheikh, and E. P. Simoncelli, "Image quality assessment: from error visibility to structural similarity," IEEE Trans. Image Process. **13**, 600–612 (2004).